# Infantile Rhabdomyosarcomas With *VGLL2* Rearrangement Are Not Always an Indolent Disease

## *A Study of 4 Aggressive Cases With Clinical, Pathologic, Molecular, and Radiologic Findings*

*Joanna Cyrta, MD, PhD,* Arnaud Gauthier, MD,* Marie Karanian, MD,† Andre F. Vieira, PhD,* Liesbeth Cardoen, MD,‡ Nina Jehanno, MD,§ Mégane Bouvet, BSc,‖ Corinne Bouvier, MD, PhD,¶ Mina Komuta, MD, PhD,#** François Le Loarer, MD, PhD,†† Daniel Orbach, MD, PhD,‡‡ Angélique Rome, MD,§§ Véronique Minard-Colin, MD, PhD,‖‖ Bénédicte Brichard, MD, PhD,¶¶ Claire Pluchart, MD, PhD,## Estelle Thebaud, MD,*** Marleen Renard, MD, PhD,¶¶ Stéphanie Pannier, MD, PhD,††† Hervé Brisse, MD, PhD,‡ Philippe Petit, MD,‡‡‡ Camille Benoist, PhD,§§§ Gudrun Schleiermacher, MD, PhD,‡‡ Birgit Geoerger, MD, PhD,‖‖ Anne Vincent-Salomon, MD, PhD,* Paul Fréneaux, MD,* and Gaëlle Pierron, PhD‖*



**Abstract:** *VGLL2*-rearranged rhabdomyosarcomas (RMS) are rare low-grade tumors with only favorable outcomes reported to date. We describe 4 patients with *VGLL2*-rearranged RMS confirmed by molecular studies, who experienced local progression and distant metastases, including 2 with fatal outcomes. Tumors were diagnosed at birth (n = 3) or at 12 months of age (n = 1), and were all localized at initial diagnosis, but unresectable and therefore managed with chemotherapy and surveillance. Metastatic progression occurred from 1 to 8 years from diagnosis (median, 3.5 y). Three patients experienced multimetastatic spread and one showed an isolated adrenal metastasis. At initial diagnosis, 3 tumors displaying bland morphology were misdiagnosed as fibromatosis or infantile fibrosarcoma and initially managed as such, while 1 was a high-grade sarcoma. At relapse, 3 tumors showed high-grade morphology, while 1 retained a low-grade phenotype. Low-grade primary tumors showed only very focal positivity for desmin, myogenin, and/or MyoD1, while high-grade tumors were heterogenously or diffusely positive. Whole-exome sequencing, performed on primary and relapse samples for 3 patients, showed increased genomic instability and additional genomic alterations (eg, *TP53*, *CDKN2A*/*B*, *FGFR4*) at relapse, but no recurrent events. RNA sequencing confirmed that high-grade tumors retained *VGLL2* fusion transcripts and transcriptomic profiles consistent with *VGLL2*-rearranged RMS. High-grade samples showed a high expression of genes encoding cell cycle proteins, desmin, and some developmental factors. These 4 cases with distinct medical history imply the importance of complete surgical resection, and suggest that RMS-type chemotherapy should be considered in unresectable cases, given the risk of high-grade transformation. They also emphasize the importance of correct initial diagnosis.

**Key Words:** pediatric cancer, rhabdomyosarcoma, congenital rhabdomyosarcoma, infantile rhabdomyosarcoma, spindle-cell rhabdomyosarcoma, *VGLL2*, *NCOA2*, *CITED2*

(*Am J Surg Pathol* 2021;00:000–000)

From the Departments of *Pathology; ‡Imaging; §Nuclear Medicine; §§§Biopathology and Genetics; ‖Genetics Unit, Department of Tumor Biology; ‡‡SIREDO Oncology Center (Care, Innovation and Research for Children and AYA With Cancer), Curie Institute, PSL Research University; †††Department of Orthopedic Surgery, University Hospital Necker-Enfants-Malades, Paris; †Department of Pathology, Lyon University Hospital, Lyon; Departments of ¶Pathology; §§Pediatric and Adolescent Hematogy and Oncology; ‡‡‡Radiology, La Timone Hospital, Aix Marseille University, Marseille; ††Department of Pathology, Bergonié Institute, Bordeaux; ‖‖Department of Pediatric and Adolescent Oncology, Gustave Roussy Cancer Campus, INSERM U1015, Paris-Saclay University, Villejuif; ***Department of Pediatric Hemato-oncology, University Hospital of Nantes, Nantes; ##Department of Paediatric Oncology/Hematology, American Hospital, University Hospital of Reims, Reims, France; Departments of #Pathology; ¶¶Pediatric Hematology/Oncology, University Hospital Saint-Luc, Catholic University of Leuven, Brussels, Belgium; and **Department of Pathology, School of Medicine, Keio University, Tokyo, Japan.

J.C. and A.G. share first co-authorship.

P.F. and G.P. share senior co-authorship.

Conflicts of Interest and Source of Funding: The MAPPYACTS trial is supported by grants from the Institut National de Cancer (INCa) through the PHRC "INCa-DGOS_8519" MERRI, the Fondation ARC, the Association Imagine for Margo, the Federation Enfants et Santé, the Société Française de lutte contre les Cancers et les leucémies de l'Enfant et l'adolescent (SFCE), and Dell. The authors have disclosed that they have no significant relationships with, or financial interest in, any commercial companies pertaining to this article.

Correspondence: Joanna Cyrta, MD, PhD Service de Pathologie, Institut Curie, 26 rue d'Ulm, Paris 75005, France (e-mail: joanna.cyrta@curie.fr).

Supplemental Digital Content is available for this article. Direct URL citations appear in the printed text and are provided in the HTML and PDF versions of this article on the journal's website, www.ajsp.com.



Congenital/infantile sclerosing and spindle-cell rhabdomyosarcomas (ssRMS) with *VGLL2* and/or *NCOA2* rearrangement represent a rare distinct subtype of rhabdomyosarcoma

(RMS).[1,2] All cases reported to date in the literature for which follow-up data are available (n = 19, median follow-up: 29 mo) have shown favorable outcomes and no metastatic events have been described.[1–6] Conversely, we identified 4 cases of *VGLL2*-rearranged RMS with several years' follow-up that showed metastatic progression, including death due to the disease in 2 cases. We show that disease progression may be accompanied by sarcomatous high-grade transformation. We also describe whole-exome sequencing (WES) and whole-transcriptome sequencing (RNA sequencing [RNA-seq]) findings in these tumors, both at diagnosis and upon progression.

## METHODS

### Patients' Clinical and Pathologic Data

The 4 patients were diagnosed between 2011 and 2018, and were treated in France and in Belgium. Clinical data were extracted from medical records. Diagnostic pathology slides were retrieved from respective pathology departments and centrally reviewed. Informed written consent for WES and RNA-seq was obtained from parents of the 3 children for whom it was performed (2 as part of the European Precision Medicine Pediatric Oncology Program MAPPYACTS, trial reference: NCT02613962, institutional review board approval reference: 2015-A00464-45, and 1 in a systematic diagnostic setting).

### WES and Analysis

WES was performed on fresh-frozen tissue from 3 primary tumor samples and 4 relapsed tumor samples from three patients, and on matched normal DNA (blood). WES for 2 tumor samples at relapse was performed as part of MAPPYACTS and for all the other samples, as part of this research study. DNA was extracted from cells after 2-hour treatment with proteinase K and 1 hour with RNAse A, using the phenol/chloroform and Phase Lock Gel Light procedure (Eppendorf, Hamburg, Germany); 500 ng to 1 µg of DNA was used to prepare 100 bp paired-end multiplexed WES libraries following the SureSelect Agilent-XTHS Clinical research V2 protocol (Agilent Technologies, Carlsbad, CA). Libraries were sequenced on the NextSeq 500 System (Illumina Inc., San Diego, CA) at a target coverage depth of 30× for germline and 100× for somatic DNA. Following sequencing, raw reads were mapped to the reference human genome assembly GRCh37/hg19. Bowtie2 (2.1.0) was used for global alignment allowing one mismatch in a seed size of 22; only the best alignment was kept. Following GATK best practices, BAM files were cleaned with Picard (2.18.13: SortSam, MarkDuplicates, and AddOrReplaceReadGroups) and GATK (3.8-1-0: RealignerTargetCreator, IndelRealigner, BaseRecalibrator, and PrintReads). Coverage was analyzed with GATK DepthOfCoverage using 20 as base quality and 6 as mapping quality, as used for variant calling. Variants were called with GATK (3.8-1-0) HaplotypeCaller and UnifiedGenotyper with the same quality parameters mentioned before. The results of calling were combined, taking preferentially the output of HaplotypeCaller in case of variants called by both tools. The variants were annotated with annovar-2018Apr16 (RefSeq, COSMIC v86, 1000g2014Oct, Esp6500si, ljb26_all). Variants with frequency > 0.1%, in the general population, a low Phred quality score (<30), located within intronic regions (except splice acceptor and donor sites) or synonymous (except those with a COSMIC ID) were filtered out. Copy number profiles were generated with a combination of VarScan (v2.4.3) and DNAcopy (v1.52.0), FREEC and Sequenza (v3.0.0). Following variant calling, images for all variants were generated with IGV (v2.4.14) and were visually inspected, reviewed, and validated by clinical biologists.

### RNA-seq and Analysis

RNA-seq was performed on 3 primary tumor samples and on 4 relapsed tumor samples from 3 patients; it was performed as part of MAPPYACTS for 2 samples, as part of an institutional project for characterizing unclassified sarcomas for 3 samples,[7] as part of this study for 1 sample, and as part of a diagnostic workup for 1 sample. Total RNA was extracted from fresh-frozen tumor tissue with the Trizol/chloroform method (Thermo Fisher Scientific, Carlsbad, CA) and qualified with fragment analysis by TapeStation 4200 (Agilent Technologies). Libraries were prepared with TruSeq mRNA stranded library kits (Illumina Inc.). To start with 1 µg total RNA per sample was purified, reverse transcribed, fragmented, indexed and amplified to make RNA libraries. Libraries were sequenced over 2×150 bp with a 500 High Output v2 on NextSeq. 500 (Illumina Inc.). Expression data were generated using Star Aligner (V2.5.3a) and count matrixes using FeatureCount (V1.6.0). The count matrixes were normalized as transcripts per million. Data were used for clustering analysis (Ward method and Spearman or Pearson correlation with or without internal quantile range) and for boxplot generation. For principal component analysis, genes with at least 0.5 transcripts per million in 20% of all samples were kept for further analysis. Analyses were performed in R software and clustering by principal component analysis was performed with the prcomp function. Fusion analysis was performed from fastq files with 2 approaches: (1) a targeted analysis using dedicated reference fusion sequences implemented with known fusions of each tumor type and (2) an exploratory analysis using 5 fusion finder tools (TopHat fusion v2.0.6, Defuse V0.6.0, StarFusion V2.5.3, Fusion Catcher v1.00, and FusionMap). Both approaches were combined for interpretation of results.

## CLINICAL CASES

### Patient 1

This boy (Fig. 1A) was born in 2012 at term after a spontaneous dizygotic twin pregnancy. A localized right shoulder mass was detected on antenatal ultrasound. The twin sister was and remains healthy. Magnetic resonance imaging (MRI) performed on day 2 of life showed a well-defined soft-tissue mass of the right upper arm and the axillary region with neurovascular encasement, measuring 90 mm in largest tumor diameter (Fig. 1B). Core needle biopsy of the mass on day 5 of life showed a moderately

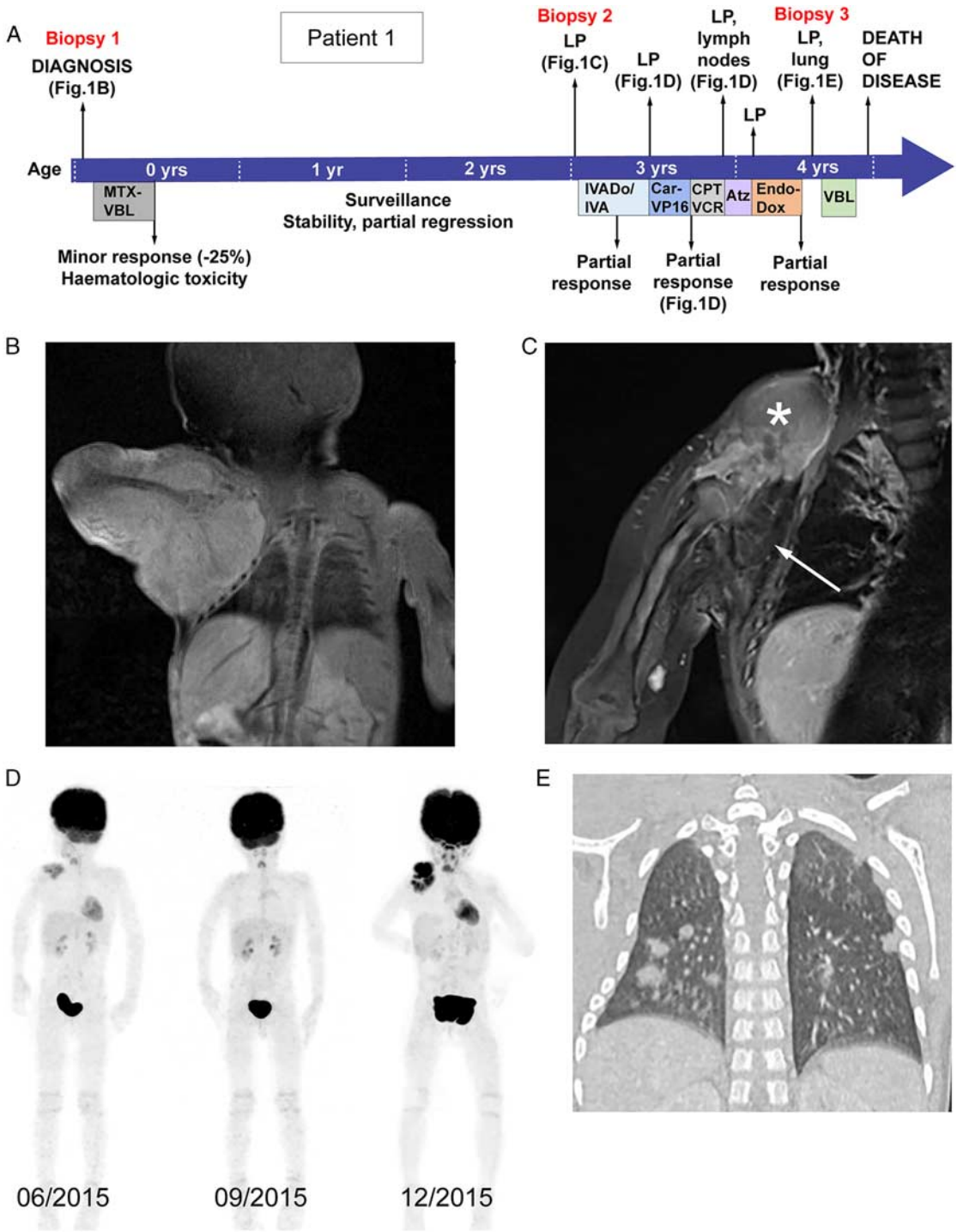


**FIGURE 1.** Clinical history and selected imaging for patient 1. A, Clinical timeline. B, Coronal proton density–weighted fat-saturated MRI at diagnosis, showing a soft-tissue mass of the right shoulder girdle. C, Coronal T1-weighted contrast-enhanced MRI, showing the residue (arrow) with tumor progression in the upper portion of the lesion (asterisk). D, Whole-body $^{18}$F-FDG PET images at 3 different timepoints; *left:* upon local progression on the IVA regimen—moderate uptake of the right shoulder lesion, maximum standardized uptake value ($SUV_{max}$) = 3.6; *middle:* after 3 doses of carboplatin-etoposide—excellent metabolic response with resolution of uptake, barely distinguishable from the surrounding background, $SUV_{max}$ = 1.4; *right:* 3 months later—local progression with a highly metabolic lesion of the right shoulder area, $SUV_{max}$ = 11, and homolateral supraclavicular lymph node extension. E, Coronal computed tomography image showing bilateral lung metastases. Atz indicates atezolizumab; Car-VP16, carboplatin-etoposide; CPT-VCR, irinotecan-vincristine; Endo-Dox, endoxan-doxorubicin; IVA, ifosfamide-vincristine-actinomycin D; IVADo, ifosfamide-vincristine-actinomycin D-doxorubicin; LP, local progression; MTX-VBL, methotrexate-vinblastine; VBL, vinblastine.

cellular, fascicular lesion composed of spindle cells arranged in a fibrous stroma, without nuclear atypia or mitotic activity. A multiplex reverse transcription-polymerase chain reaction (RT-PCR) panel performed at the time (Supplemental Digital Content 1—Table ST1, http://links.lww.com/PAS/B96) was negative for common sarcoma-associated fusion transcripts. Thus, diagnosis of congenital fibromatosis was favored. A limb-sparing surgical resection was not possible because of the invasion of the shoulder girdle and the neurovascular bundle. Because of severe shoulder limitation, chemotherapy with methotrexate-vinblastine was initiated, but was discontinued after 3 months due to poor hematologic tolerance and no significant tumor volume decrease. The residual mass remained stable in volume throughout several years, and evolved into a fibrous soft-tissue residue. However, at 3 years of age, a volume increase, associated with a higher T2 signal and heterogenous contrast uptake of the upper portion of the tumor residue was observed (Fig. 1C). Biopsy of the upper portion of the shoulder mass showed different features from the initial sample, with obvious high-grade sarcomatous transformation (ie, a highly cellular tumor composed of spindle to round tumor cells arranged in sheets, showing severe nuclear atypia and numerous mitoses). RNA-seq performed on the initial diagnostic biopsy and on the biopsy at progression identified an identical *VGLL2-NCOA2* fusion transcript (exon 2 to exon 13) in both samples. The patient was treated with several chemotherapy regimens, including conventional alkylating agent-anthracycline regimens, which resulted in partial response, followed by progression (Figs. 1A, D). Local progression was observed on treatment with the anti–programmed death-ligand 1 antibody atezolizumab during 3 months within a clinical trial (NCT02541604).[8] Fifteen months after the onset of locoregional progression, the patient suffered metastatic extension to the lungs (Fig. 1E). His health condition deteriorated rapidly, and the boy deceased 5 months later.

## Patient 2

This girl (Fig. 2A) was born in 2011 at term, after normal antenatal ultrasounds. At birth, physical examination showed a mass on the left arm. MRI (Fig. 2B) objectified a heterogenous soft-tissue mass of the left arm and the axillary region, measuring 80 mm in largest diameter, infiltrating the glenohumeral joint and encasing the axillary neurovascular bundle. Core needle biopsy showed a spindle-cell tumor with focal atypia and focal positivity for smooth muscle actin. The initially favored diagnosis was infantile fibrosarcoma, but no *ETV6* rearrangement was found by fluorescence in situ hybridization, and a multiplex RT-PCR panel performed at that time (Supplemental Digital Content 1—Table ST2, http://links.lww.com/PAS/B97) was negative for sarcoma-associated fusion transcripts. The subsequently performed RNA-seq showed a *VGLL2-NCOA2* fusion transcript (exon 2 to exon 13) and the tumor was reclassified as *VGLL2*-rearranged RMS. The tumor was localized, but considered unresectable and the patient was initially observed. At 3 months of age, the mass had increased in size to 120 mm, with abolished upper limb mobility. The patient received chemotherapy with vincristine-actinomycin D for 12 months. An evolution toward fibrosis was observed, but with only a slight decrease in tumor size and the mass remained unresectable. The mass remained stable for several years. At the age of 8 years, pain symptoms and tumor volume increased (Fig. 2C). Fluorine-18 fluorodeoxyglucose positron emission tomography/computed tomography ($^{18}$F-FDG PET/CT) showed hypermetabolism of the shoulder tumor (maximum standardized uptake value = 6.9), hypermetabolic regional supraclavicular lymph nodes, multiple bone lesions in the vertebra, pelvis and scapulae and lung metastases (Fig. 2D). Surgical biopsy of the shoulder mass showed histologic features different from the initial biopsy with increased cellularity, marked nuclear pleomorphism, high mitotic activity, and tumor necrosis. The patient was started on chemotherapy with the vincristine-doxorubicin-cyclophosphamide/ifosfamide-etoposide (VDC/IE) regimen, showing partial radiologic and complete metabolic response of the primary mass and metastases after 7 cycles. She currently remains on treatment 7 months after treatment initiation.

## Patient 3

This girl born in 2017 presented at 12 months of age, after an uneventful neonatal period, with a painless right dorsal paravertebral mass. MRI showed an intramuscular mass measuring 60 mm in largest dimension, with intrathoracic extension, minimal intracanalar extension, and erosion of nearby vertebrae resulting in T3 and T4 vertebrae planae. Biopsy showed a spindle-cell neoplasm with atypia and numerous mitoses, strong and diffuse expression of MyoD1, and patchy positivity for myogenin; it was negative for *FOXO1* rearrangement and *MYOD1* mutation. A *VGLL2-CITED2* fusion transcript (exon 2 to exon 2) was detected by RNA-seq on formalin-fixed, paraffin-embedded material. Chemotherapy with ifosfamide-vincristine-actinomycin D (IVA) was started at 14 months of age for a total of 9 cycles, achieving complete radiologic response on MRI after 6 cycles, and was followed by maintenance chemotherapy with low-dose vinorelbine-cyclophosphamide. No local treatment was performed because of complete local response and young age limiting radiotherapy. During the third cycle of maintenance treatment, at 24 months of age, the child presented local relapse, with an intramuscular dorsal mass measured at 45 mm and showing heterogenous enhancement on MRI. A new biopsy identified a high-grade RMS with an elevated Ki-67 index (50%). Salvage chemotherapy with the VIT regimen (vincristine-irinotecan-temozolomide) was started, resulting in stable disease, followed by proton therapy for a total dose of 41.4 Gy and VAC (vincristine-D actinomycin-cyclophosphamide) regimen, with minor response. Complete surgery of the residual disease was performed next and showed viable tumor cells on the resection specimen. VAC chemotherapy was resumed 1 month after surgery, but after one cycle (at 2 y and 8 mo of age), the child showed rapid clinical deterioration, leading to the discovery of multiple lung metastases, and died of disease 1 month later.

## Patient 4

This girl born in 2015 presented at birth with right inferior limb monoplegia. MRI demonstrated a left lumbar paravertebral soft-tissue mass with left

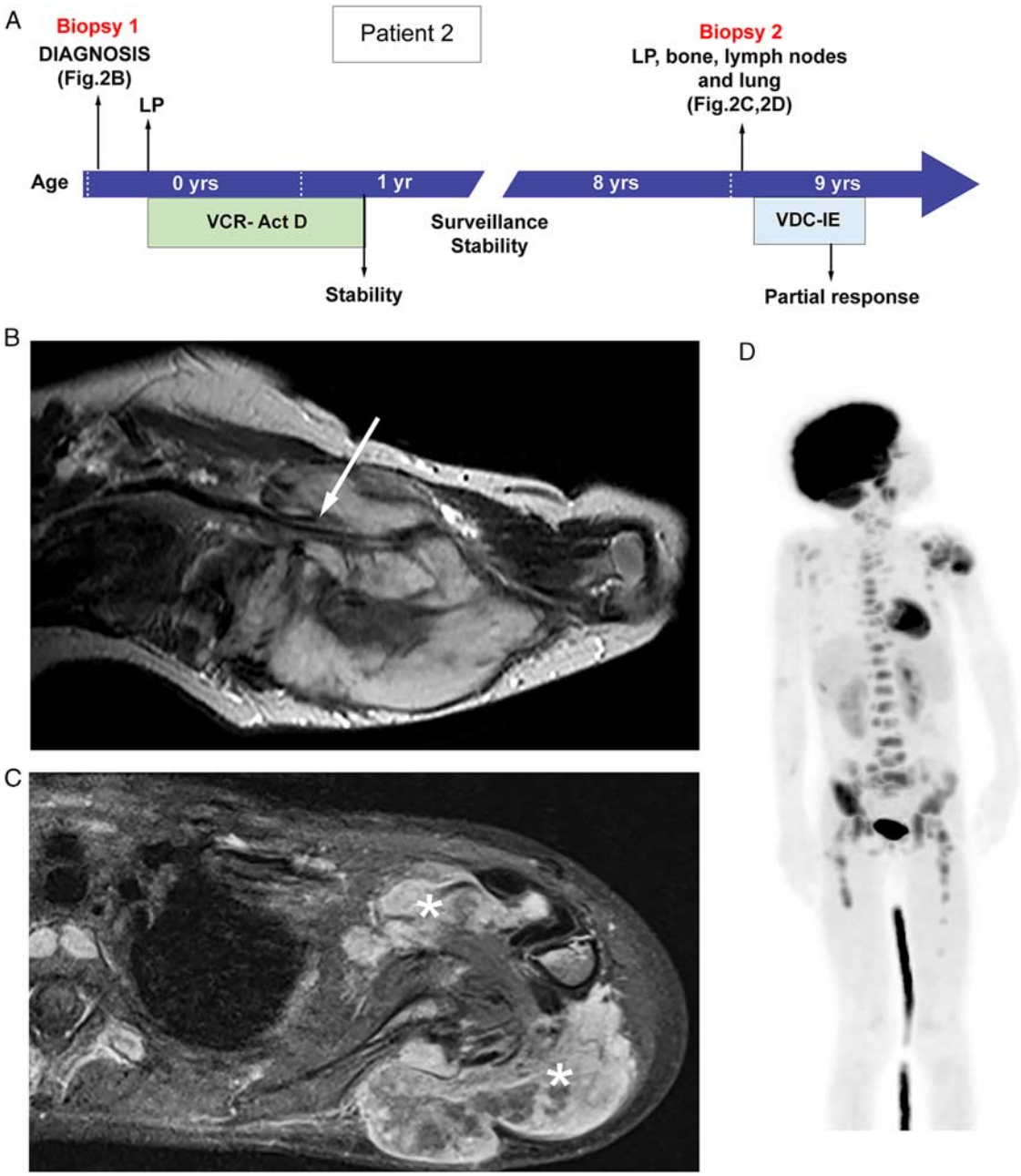


**FIGURE 2.** Clinical history and selected imaging for patient 2. A, Clinical timeline. B, Axial oblique T2-weighted MRI, centered on the axillary region, shows a soft-tissue mass of left arm and axillary region encasing the axillary neurovascular bundle (arrow). C, Axial T1-weighted contrast-enhanced MRI, showing tumor progression in the upper portion of the lesion (asterisks). D, Whole-body $^{18}$F-FDG PET/CT images showing an intense metabolic uptake of the primary left shoulder lesion associated with locoregional axillary lymph node extension, pulmonary metastases, and diffuse bone infiltration. $^{18}$F-FDG PET/CT indicates luorine-18 fluorodeoxyglucose positron emission tomography/computed tomography; LP, local progression; VCR-Act D, vincristine-actinomycin D; VDC/IE, vincristine-doxorubicine-cyclophosphamide/ifosfamide-etoposide.

retroperitoneal and intracanalar extension (dumbbell tumor) (Supplemental Digital Content 2—Fig. S1, http://links.lww.com/PAS/B98). Core needle biopsy showed a spindle-cell tumor infiltrating the muscle, without atypia or mitoses. Focal positivity for desmin and myogenin was noted. A multiplex RT-PCR panel performed at the time (Supplemental Digital Content 1—Table ST1, http://links.lww.com/PAS/B96) was negative for common sarcoma-associated fusion transcripts, and diagnosis of fibromatosis was initially favored. The patient received steroids, but the tumor increased in size. Chemotherapy with methotrexate-vinblastine led to tumor stabilization. At 10 months of age, the

patient underwent partial excision of the mass (R2: resection with gross residual disease) and RNA-seq showed a *VGLL2-NCOA2* fusion transcript (exon 3 to exon 13). Diagnosis was therefore corrected to ssRMS. The patient did not receive further adjuvant chemotherapy and was placed on active surveillance. At the age of 4 years, a new lesion of the left adrenal gland appeared while the remaining primary tumor was stable. $^{18}$F-FDG PET/CT tomography showed hypermetabolism of the new adrenal mass, no hypermetabolism of the residual primary, and no other distant lesion. Coelioscopic biopsy confirmed a metastatic ssRMS with a *VGLL2-NCOA2* fusion transcript on RNA-seq. The patient received 3 cycles of IVA, leading to a 78% decrease in adrenal lesion and no change of the primary tumor residue on MRI. She then underwent surgical resection of the adrenal lesion (complete resection, R0) and of the residual primary tumor (microscopically positive margins, R1), followed by 4 additional cycles of IVA and by radiation treatment to the adrenal tumor bed (50.4 Gy in 28 fractions). She remains in second complete remission 8 months after surgery.

## HISTOMORPHOLOGY

Pathology features of the primary tumors and tumors at relapse are compared in Figure 3. In patients 1 and 2, the primary tumor displayed the classic low-grade spindle-cell morphology of ssRMS; conversely, samples at relapse in patients 1 and 2 showed features of high-grade transformation: increased cellularity, nuclear pleomorphism, and brisk mitotic activity; extensive tumor necrosis was also seen in the relapse of patient 2. In patient 3, high-grade sarcomatous morphology was seen both at diagnosis and upon relapse. Last, in patient 4, both primary tumor and metastasis showed bland low-grade morphology, with no histologic evidence of high-grade transformation in the adrenal metastasis.

## IMMUNOHISTOCHEMISTRY

All tumor samples (primary and relapse) from the 4 patients showed some degree of positivity for rhabdomyoblastic markers (desmin, myogenin, and/or MyoD1), but the intensity and extent of these stainings varied greatly between samples. Immunohistochemistry (IHC) results for all samples are summarized in Table 1. Representative stainings are shown in Figures 4 and 5.

## GENOMIC AND TRANSCRIPTOMIC FINDINGS

WES was performed for patients 1, 2, and 4 on primary tumors and tumors at relapse.

The 3 primary samples with low-grade morphology showed remarkable genomic stability (Fig. 6), with genomic indexes (GIs) of GI = 2, GI = 3 and GI = 1, respectively. Conversely, samples after high-grade progression acquired copy number alterations and showed an increased GI (patient 1—relapse 1: GI = 12.5, patient 1—relapse 2: GI = 18.8, patient 2—relapse: GI = 57.3), and whole-genome duplication was seen in the relapse sample of patient 2. Interestingly, some degree of genomic instability was also observed in the metastatic sample of patient 4 (GI = 5.3), despite the lack of morphologic high-grade transformation. The tumor mutation burden was extremely low in all samples (< 1 variant/Mb in every sample), including high-grade samples (Supplemental Digital Content 1—Table ST3, http://links.lww.com/PAS/B99).

WES did not identify a common genomic event associated with disease progression across all patients. However, several genomic alterations in known or putative cancer genes, specific to each patient, were detected.

In patient 1 (Supplemental Digital Content 1—Tables ST4, http://links.lww.com/PAS/B100 and ST5, http://links.lww.com/PAS/B101), relapse 2 showed a homozygous *CDKN2A/B* deletion, while no *CDKN2A/B* copy number alterations were seen in the primary tumor sample or in relapse 1. In addition, we observed a heterozygous p.Asn535Asp missense mutation in *FGFR4* (in relapse 2 only), a heterozygous p.Gln36* stop gain in *SETD2* (in relapses 1 and 2), a heterozygous p.Leu649* frameshift in *SDHA* (in relapse 1 only), a heterozygous p.Gln485* stop gain in *SMC1B* (in relapse 2 only), and several other alterations.

In patient 2, a homozygous deleterious *TP53* p.Gly245Ser hotspot mutation (variant allele fraction [VAF] = 87.8%) was observed in the sample at relapse, but not in the primary tumor (even at low VAF). Other alterations specifically found at relapse, but not in the primary tumor sample, included a homozygous p.Leu131Trp mutation in *CTNNA1*, a homozygous deletion of *FBXW10*, loss of heterozygosity of the germline *NF1* p.Arg2637Gln variant of unknown significance, and several other alterations (Supplemental Digital Content 1—Tables ST6, http://links.lww.com/PAS/B102 and ST7, http://links.lww.com/PAS/B103).

In patient 4, a heterozygous c.3609insT frameshift mutation in *RANBP2* was seen in the relapse sample, but not in the primary tumor sample, alongside a few other alterations (Supplemental Digital Content 1—Tables ST8, http://links.lww.com/PAS/B104 and ST9, http://links.lww.com/PAS/B105).

No mutations were detected in the *MYOD1* gene in any of the samples, even at low VAF.

The existence of common breakpoints and common SNVs in primary samples and in samples at relapse for each patient further supported relatedness between different samples in each patient.

Unsupervised RNA-seq-based cluster analysis of samples from this study and of 98 other tumor samples (soft-tissue spindle-cell tumors and/or RMS), confirmed that all *VGLL2*-rearranged RMS samples formed a distinct transcriptomic cluster (Fig. 7A). Importantly, tumors after high-grade transformation continued to cluster within the *VGLL2*-rearranged RMS group. However, primary tumor samples with low-grade morphology were more closely related to one another than to their matched high-grade relapse samples. Concordant results were obtained with the principal component analysis (Supplemental Digital Content 2—Supplementary Fig. S2, http://links.lww.com/PAS/B106).

Last, we queried trends in gene expression levels for selected genes related to proliferation, RMS phenotype, and/or embryonic development in samples from this study and other tumor types (Fig. 7B, Supplemental Digital

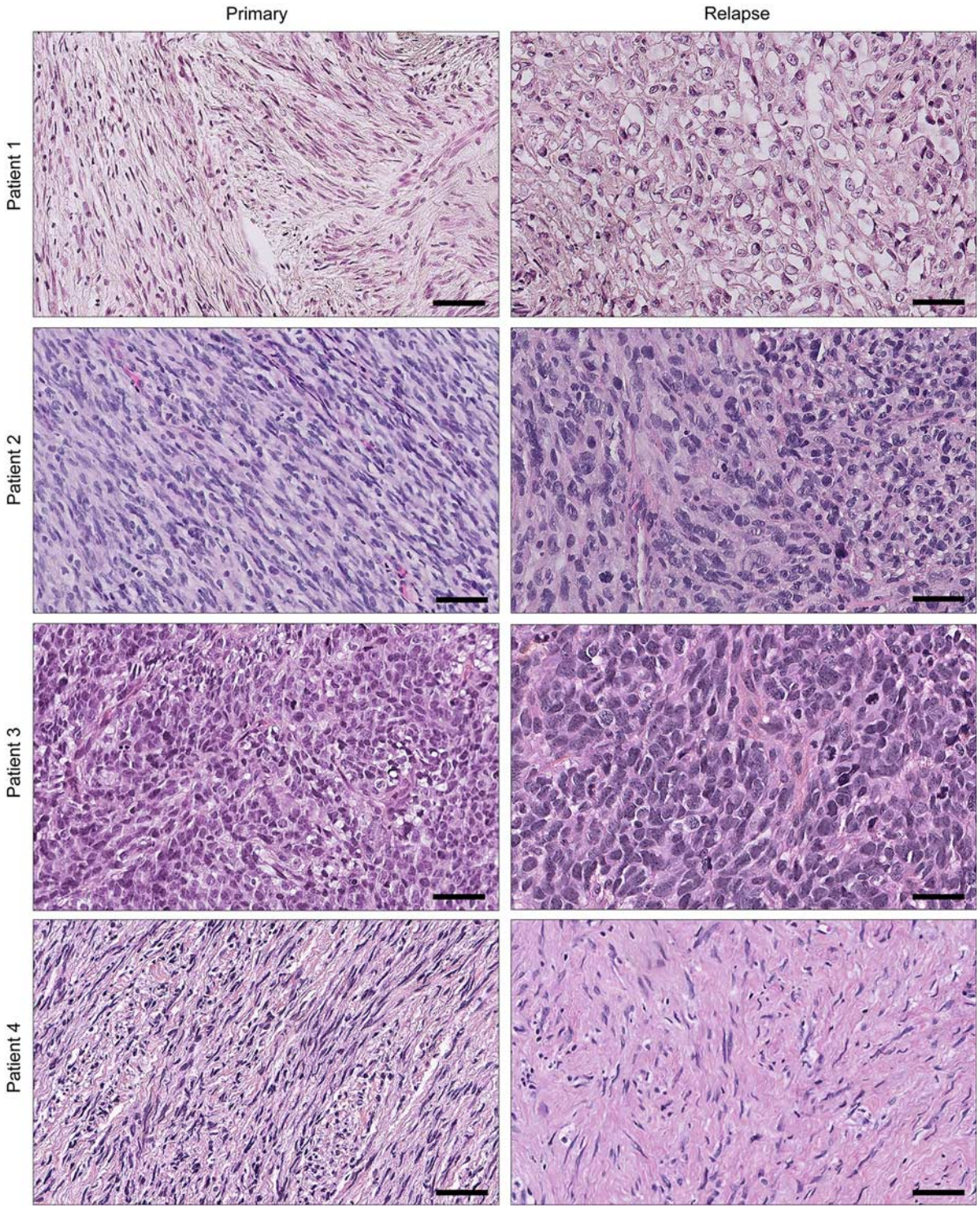


**FIGURE 3.** Comparative pathology findings at diagnosis and at relapse. Representative pathology images of tumors at diagnosis and upon progression are shown for the 4 patients. Patients 1 and 2: bland, spindle-cell morphology at initial diagnosis and high-grade morphology at progression; patient 3: high-grade morphology in both the primary tumor and the tumor at progression; patient 4: bland spindle-cell morphology in both the primary tumor and the adrenal metastasis. Hematoxylin-eosin-saffron stain (scale bar: 50 μm).

Content 2—Supplementary Fig. S3, http://links.lww.com/PAS/B107). The 3 *VGLL2*-rearranged RMS samples with high-grade morphology showed a tendency toward high expression of *DES* (desmin), *VGLL2* and *NCOA2*. They also displayed relatively high expression of genes related to cell cycle progression, including genes encoding cyclins

**TABLE 1.** Summary of IHC Findings

| | Patient 1 | | Patient 2 | | Patient 3 | | Patient 4 | |
|---|---|---|---|---|---|---|---|---|
| | Primary | Relapse | Primary | Relapse | Primary | Relapse | Primary | Metastasis |
| IHC Marker | Low Grade | High Grade | Low Grade | High Grade | High Grade | High Grade | Low Grade | Low Grade |
| Desmin | − | ++ | + | +++ | +++ | +++ | − | ++ |
| Myogenin | +/− | + | ++ | +++ | +++ | +++ | + | ++ |
| MyoD1 | + | + | NA | NA | +++ | +++ | NA | ++ |
| Ki-67 | 15%-20% | 70% | 20% | NA | NA | NA | 20% | NA |
| SMA | − | − | + | +++ | NA | NA | NA | ++ |
| h-caldesmon | − | − | NA | NA | NA | NA | NA | − |
| S100 | − | − | − | − | NA | NA | − | − |
| CD34 | − | − | − | − | NA | NA | NA | NA |
| Pankeratin | − | − | − | − | NA | NA | NA | NA |

− indicates negative; +/−, very rare positive cells; +, focal positivity; ++, heterogenous (patchy) positivity; +++, diffuse positivity; NA, not performed or not available; SMA, smooth muscle actin.

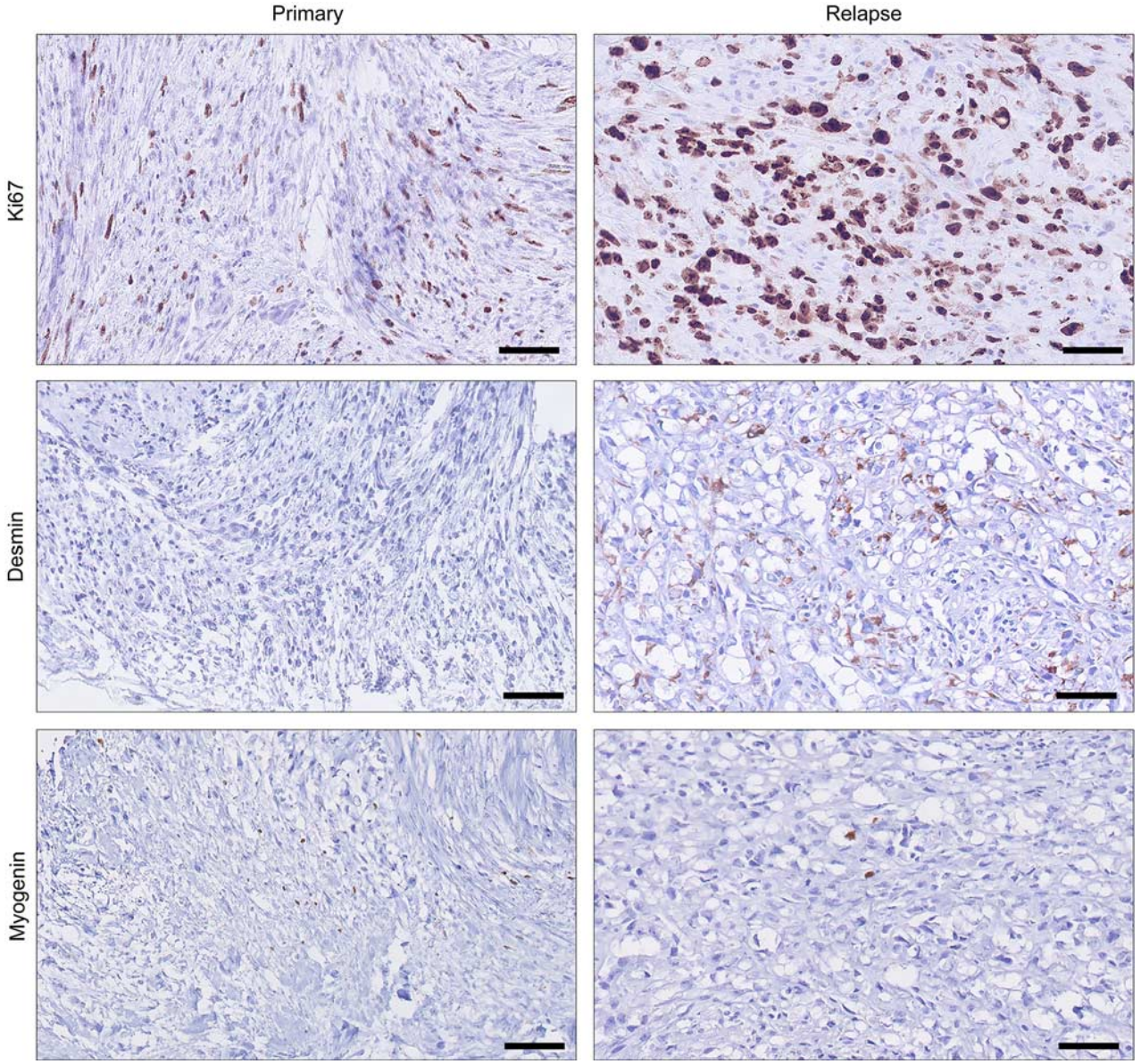


**FIGURE 4.** IHC findings in samples from patient 1. Scale bar: 50 μm.

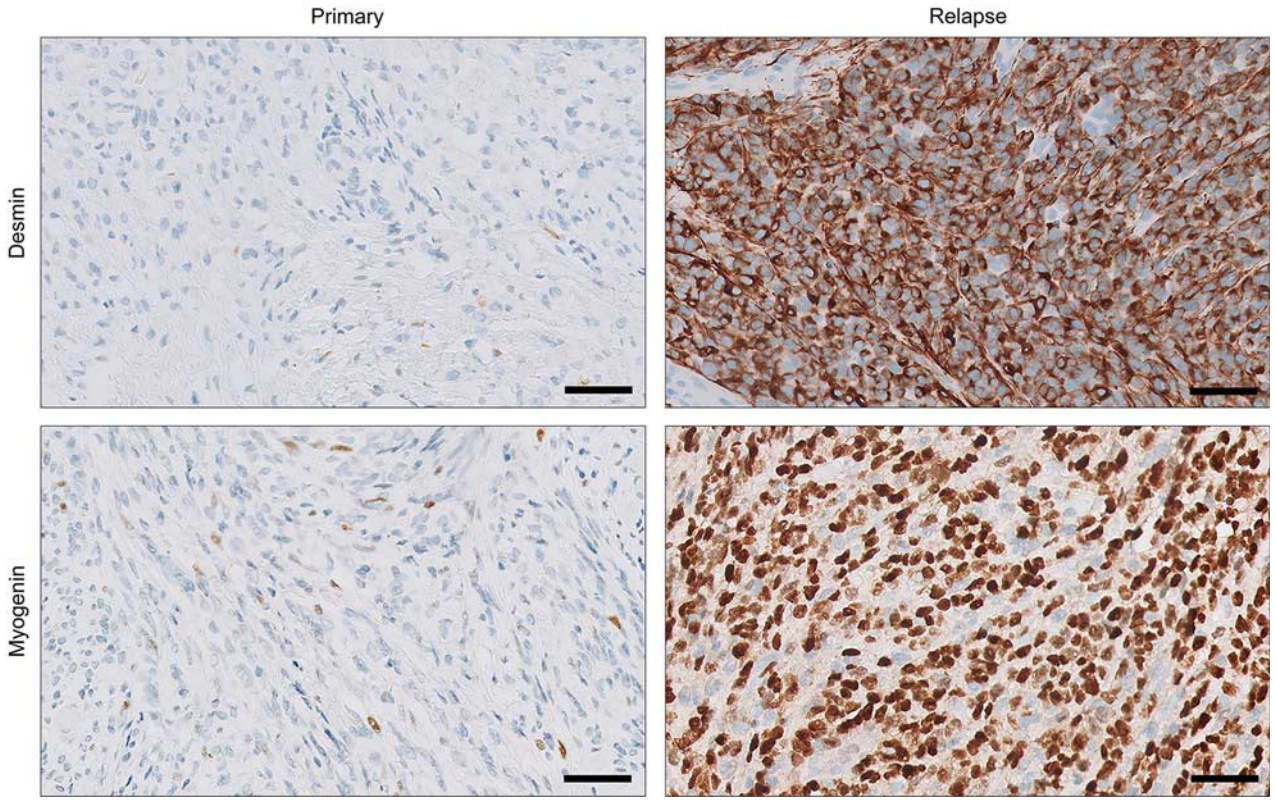


**FIGURE 5.** IHC findings in samples from patient 2. Scale bar: 50 μm.

(*CCNA2*, *CCNB1*) and Aurora kinases (*AURKA*, *AURKB*). In addition, they showed a tendency toward high expression of several transcription factors related to cell fate determination (eg, *SOX15*, *PAX6*, *FOXP2*), and relatively low expression of some other morphogenic factors (eg, *BMP6*).

Of note, based on the cluster analysis and on the expression levels of selected genes, the metastatic sample from patient 4 (which retained low-grade morphology) showed transcriptomic features that were somewhat intermediate between low-grade primary samples and samples on high-grade relapse (Figs. 7A, B).

## DISCUSSION

Despite their shared rhabdomyoblastic phenotype, RMS represent a heterogenous group of tumors, which encompasses well-characterized subtypes—embryonal RMS and alveolar RMS—and also emerging entities.[9] As such, sclerosing and spindle cell RMS were recognized as a stand-alone RMS subtype by the WHO 2013 classification and confirmed in the WHO 2020 classification.[10] Recent molecular advances allowed to subdivide this subgroup even further, by identifying at least 3 distinct entities: ssRMS with *MYOD1* mutations, ssRMS with rearrangements of vestigial-like family member 2 (*VGLL2*) and/or nuclear receptor coactivator (*NCOA2*), and intraosseous spindle cell RMS with *TFCP2* or *NCOA2* rearrangements. RMS with *MYOD1* mutations can be seen at any age above 1 year and follow an aggressive clinical course.[9,11] Conversely, RMS with *VGLL2* and/or *NCOA2* rearrangements are mainly congenital or diagnosed in infants and are classically thought to show good prognosis, with no unfavorable outcomes reported to date.[1–6] Transcriptome-based cluster analyses further support the fact that ssRMS with *VGLL2* and/or *NCOA2* rearrangements are distinct from other types of RMS[6,7] (Fig. 7A).

The classically described pathology features of ssRMS with *VGLL2* and/or *NCOA2* gene rearrangements include low-grade spindle-cell morphology with fascicular and sometimes herringbone architecture, and relatively uniform tumor cells, showing elongated, "wavy" nuclei with fine chromatin, occasional hyperchromasia and inconspicuous nucleoli[1,2] (Supplemental Digital Content 2—Supplementary Fig. S4, http://links.lww.com/PAS/B108). Tumor cells do not display significant pleomorphism or anaplasia, although some mitotic activity may be seen.[3,5] They tend to infiltrate within the skeletal muscle,[2] which was also observed in our cases, and to encase neurovascular structures (Fig. 1B, 2B). Detection of a fusion transcript associated with this subtype supports the diagnosis. *VGLL2*, which encodes a transcriptional cofactor of skeletal muscle differentiation,[12] is the most frequently reported 5′ partner, followed by *TEAD1* and *SRF*. *NCOA2* and *CITED2* are the 2 possible 3′ partners described to

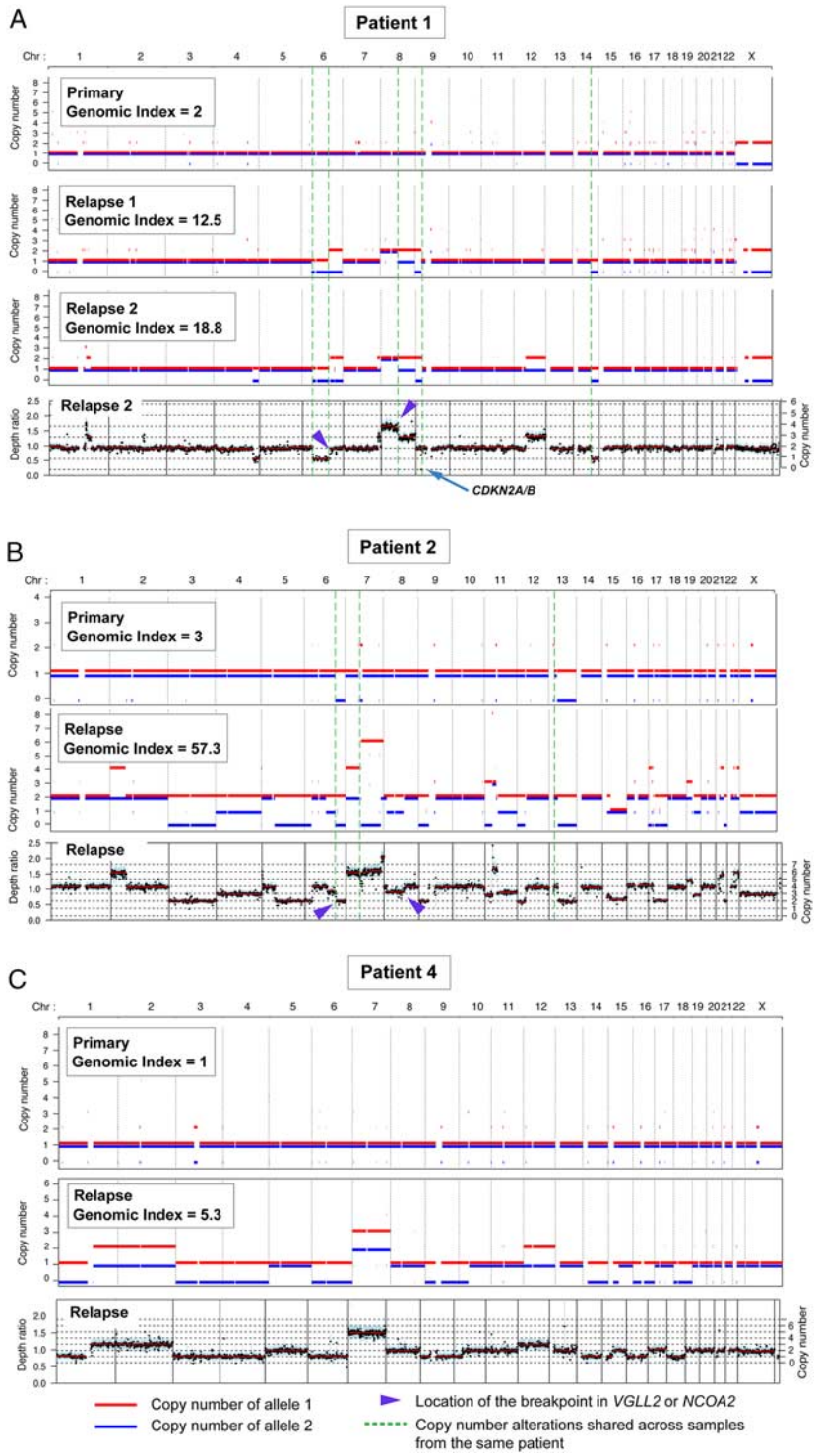


**FIGURE 6.** Comparative tumor copy number variation profiles at diagnosis and at relapse as assessed by WES in tumor samples from patients 1 (A), 2 (B), and 4 (C).

date; they encode transcriptional coactivators.[13] No morphologic differences seem to exist between ssRMS with those different fusion types[2] and it is yet unknown whether they show biological singularities. However, the *VGLL2-NCOA2* fusion is sufficient for tumorigenesis in a zebrafish model.[14] Of note, some of the above genes are also implicated in fusion events in other types of RMS, albeit with different partners.[15–17]

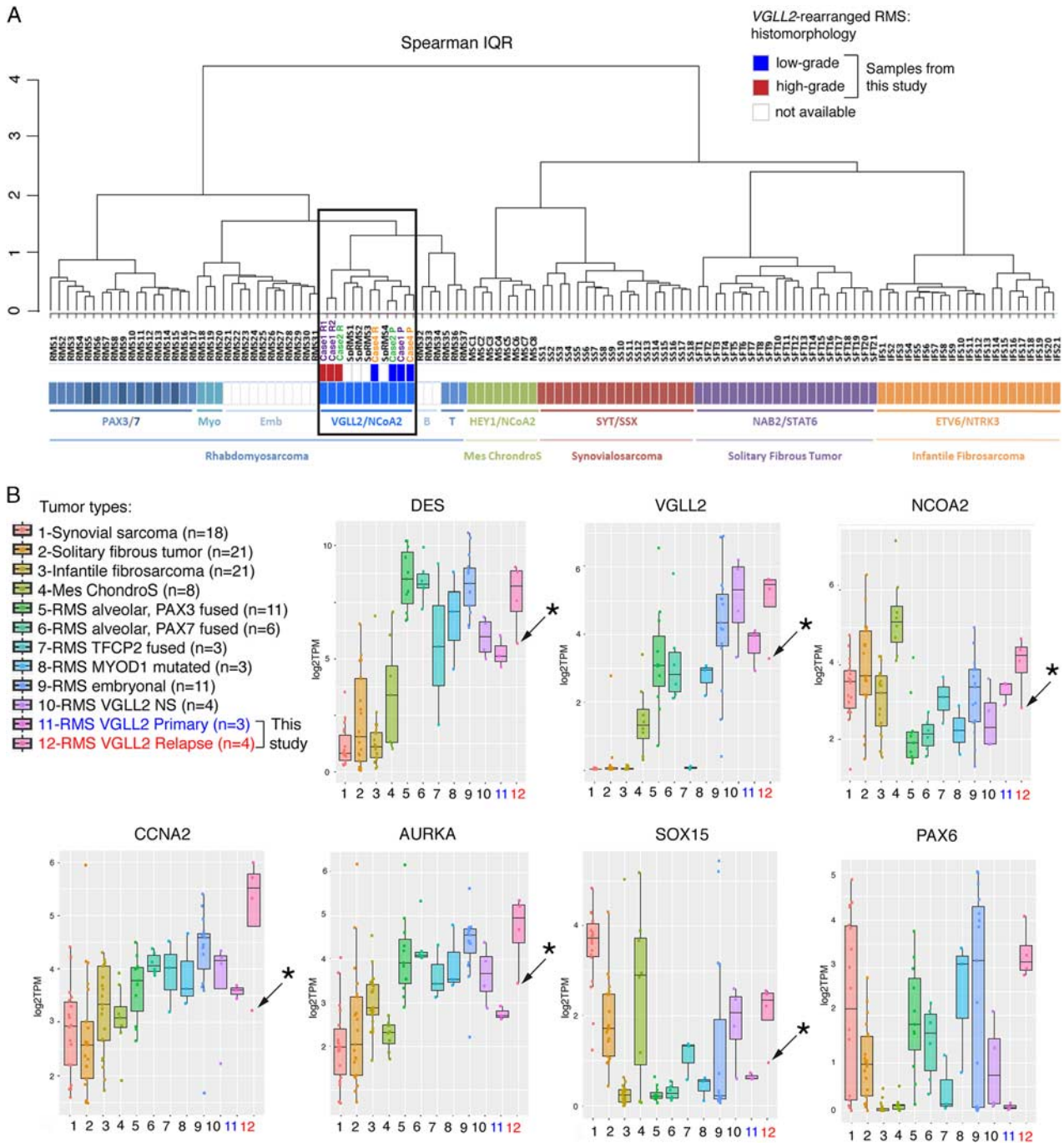


**FIGURE 7.** Transcriptomic findings (RNA-seq) in tumors from patients 1, 2, and 4. A, Unsupervised cluster analysis, including *VGLL2*-rearranged RMS (7 samples from this study and 4 other samples) and several other types of soft-tissue spindle-cell tumors and/or RMS. B, Expression levels ($log_2$TPM) of selected genes in samples from this study and in several other tumor types; boxplot representation (median, SD). The asterisk indicates the low-grade metastatic sample from patient 4. B indicates botryoid; RMS; Emb, embryonal RMS; IQR, interquartile range; MesChondroS, mesenchymal chondrosarcoma; Myo, *MYOD1*-mutated RMS; NS, morphology not specified (not available); T, RMS with *TFCP2* fusions.

Survival data in ssRMS reported before the discovery of *VGLL2*/*NCOA2* rearrangements and *MYOD1* mutations are difficult to interpret.[18,19] In more recent studies, follow-up information was available for 19 cases of ssRMS with a documented *VGLL2* and/or *NCOA2* rearrangement[2–6] (Supplemental Digital Content 1—Tables ST10, http://links.lww.com/PAS/B109). With a median follow-up of 29 months (range, 7 mo to 13 y), 2

patients experienced local recurrence,[2] but no metastatic events were reported, and all patients were alive with no evidence of disease at follow-up. Three additional, unpublished patients with *VGLL2*-rearranged RMS were identified in our institution's database (Supplemental Digital Content 1—Table ST11, http://links.lww.com/PAS/B110); they showed favorable outcome with no metastatic events and no evidence of disease at follow-up (between 5 and 7 y). Overall, previous observations implied that these tumors carry a favorable prognosis, and some authors argued that patients with this tumor type could potentially be spared aggressive multimodal treatments, especially given the very young age at diagnosis.

In contrast to the above cases, we report for the first time 4 patients diagnosed with *VGLL2*-rearranged RMS who experienced local progression followed by distant metastases, including 3 cases with multimetastatic spread and 2 with a fatal outcome. Local progression manifested as the appearance of a new, rapidly growing mass emerging from the "latent" primary tumor (Fig. 1C, 2C) and was accompanied by histologic high-grade transformation (Supplemental Digital Content 2—Supplementary Fig. S5, http://links.lww.com/PAS/B111 in 2 patients. Of note, such progression could occur after prolonged clinical stability of the residue, as long as 8 years (patient 2). Metastatic sites included the lung, bone, lymph nodes, and the adrenal gland.

Two important differences in terms of clinical management need to be emphasized between these 4 distinct cases with negative outcome, and the previously published and unpublished cases with favorable outcome (Supplemental Digital Content 1—Tables ST10, http://links.lww.com/PAS/B109 and ST11, http://links.lww.com/PAS/B110). First, 12 of the 13 patients reported in the literature for whom this information was available, and 3 additional unpublished patients with favorable outcomes, underwent surgical resection of the tumor, with R0 or R1 margins (ie, no gross residual disease) achieved in most cases. Conversely, in all 4 patients reported herein, the primary tumor was initially considered unresectable. Second, most patients reported in the literature, and the 3 unpublished patients, had received RMS-type chemotherapy (VAC/IVA); conversely, 3 of the 4 patients from our study were initially treated with other, potentially suboptimal regimens, due to their tumors being at first misdiagnosed as benign or low-grade entities. Although these data need to be interpreted with caution due to the small sample size, they could imply the importance of complete surgical excision in *VGLL2*-rearranged RMS, and suggest that RMS-type chemotherapy should be considered in cases that are deemed unresectable. Importantly, resection may not always be possible without mutilating surgery, due to the propensity of these tumors to vast locoregional extension, as illustrated in this study.

Another essential point raised by these observations is the importance of achieving a correct initial diagnosis. Pathologists should be aware that *VGLL2*-rearranged RMS may display a spectrum of morphologies,[2,7] which can range from a deceptively bland, fibromatosis-like appearance (eg, patient 1—primary) to high-grade sarcoma. Differential diagnoses in this age group include infantile fibromatosis, myofibroma/myofibromatosis and infantile fibrosarcoma.[20,21] Positivity of rhabdomyoblastic markers desmin, myogenin, and/or MyoD1 on IHC may be helpful in diagnosing ssRMS, and MyoD1 has been suggested to show the highest sensitivity in this setting.[9] However, these markers are often only focally positive in ssRMS, which can be problematic on core needle biopsy. Accordingly, the 3 low-grade primary samples from our cohort (patients 1, 2, and 4) showed only focal positivity for those markers (Table 1, Figs. 4, 5). Two of these cases were initially misdiagnosed as fibromatosis, and one as infantile fibrosarcoma (although in 2 cases, the initial diagnosis predated the description of *VGLL2*-rearranged RMS as an entity in the literature). Although a relatively elevated Ki-67 index (around 20% in our cohort) could raise suspicion of ssRMS as opposed to fibromatosis or myofibroma, interpretation of Ki-67 is difficult in the neonatal period, as it can be physiologically elevated in various tissues, and its potential utility in this setting needs to be validated in a larger cohort. Overall, these examples advocate the use of systematic molecular testing in pediatric mesenchymal tumors as part of the diagnostic workup, even if microscopic presentation is seemingly straightforward, with the potential of confirming the proposed diagnosis, amending it in some cases, and identifying novel molecular alterations.[22] Given the ever-expanding landscape of tumor-associated gene fusions, which are not always included in RT-PCR panels, RNA-seq may be the strategy of choice for characterizing challenging pediatric spindle-cell tumors to avoid misdiagnosis and undertreatment.

On the opposite side of the spectrum, we show that high-grade morphology can occur in *VGLL2*-rearranged RMS through the high-grade transformation of a low-grade tumor, or be readily present at the time of diagnosis, as it was seen in patient 3. High-grade *VGLL2*-rearranged RMS were positive for rhabdomyoblastic markers on IHC and retained a transcriptomic profile consistent with *VGLL2*-rearranged RMS. High-grade sarcomatous transformation in fusion-associated pediatric tumors is not a common event, but it has been described for some entities, such as dermatofibrosarcoma protuberans.[23–25] Our WES results showed that high-grade transformation in *VGLL2*-rearranged RMS is accompanied by increased genomic instability, and a deleterious *TP53* alteration was found in the high-grade sample of patient 2, although we were not able to evidence a common genomic event associated with disease progression across the 3 patients.

After metastatic progression, in cases presented herein, conventional chemotherapy regimens showed partial, transient efficacy. Although WES results did not alter the management of patients from our study, we did identify several alterations in known cancer genes. Of note, the p.Asn535Asp variant of *FGFR4* (VAF = 38.8%), found in the second relapse biopsy of patient 1, has previously been identified in RMS and was shown to promote tumor growth and metastasis in vitro and in vivo.[26] This mutant form of FGFR4 is resistant to many tyrosine kinase inhibitors, but retains sensitivity to ponatinib.[27]

The fact that additional oncogenic alterations in cancer genes may occur in high-grade *VGLL2*-rearranged RMS suggests that next-generation sequencing may be useful in those patients to look for potential actionable alterations.

Consistent with pathology findings of increased mitotic activity in high-grade samples, RNA-seq showed high expression of genes associated with cell cycle progression in these samples. This included some putative therapeutic targets, although further studies are needed to support this hypothesis. For example, Aurora A kinase can be targeted by alisertib, which has shown a manageable toxicity profile in pediatric patients, but inconsistent single-agent activity depending on the tumor type.[28,29] High-grade *VGLL2*-rearranged RMS also showed a tendency toward high expression of some factors related to embryonic development, including the transcription factor *SOX15*, which is thought to play a role in muscle precursor cell specification and in skeletal muscle regeneration, while inhibiting differentiation of myoblasts to myotubes.[30–32] It is yet unknown which exact type of adult or embryonic tissue *VGLL2*-rearranged RMS is most closely related to, but gene expression signatures from a *VGLL2-NCOA2* zebrafish tumor model recently pointed toward transcriptomic similarities with early somitogenesis.[14]

Overall, our findings expand the current knowledge on *VGLL2*-rearranged RMS, by demonstrating their propensity for high-grade transformation. Nevertheless, they are limited by the small sample size due to the rarity of these tumors. Further studies are needed to better elucidate the clinical, histopathologic, and molecular factors associated with, and potentially predictive of, disease progression in *VGLL2*-rearranged RMS, and to investigate treatment options for patients who experience relapse. Establishing a collaborative international database with long-term follow-up should be particularly encouraged in the context of this rare disease.

## ACKNOWLEDGMENTS

*The authors acknowledge the patients and their families for participating in precision cancer care studies. The MAPPYACTS trial is supported by grants from the Institut National de Cancer (INCa) through the PHRC "INCa-DGOS_8519" MERRI, the Fondation ARC, the Association Imagine for Margo, the Federation Enfants et Santé, the Société Française de Lutte contre les Cancers et les leucémies de l'Enfant et l'adolescent (SFCE), and Dell. The Authors also thank Dr Louise Galmiche-Rolland (Department of Pathology, University Hospital of Nantes) for her help with retrieving pathology-related data for one case.*

## REFERENCES

1. Mosquera JM, Sboner A, Zhang L, et al. Recurrent NCOA2 gene rearrangements in congenital/infantile spindle cell rhabdomyosarcoma. *Genes Chromosomes Cancer*. 2013;52:538–550.
2. Alaggio R, Zhang L, Sung YS, et al. A molecular study of pediatric spindle and sclerosing rhabdomyosarcoma: identification of novel and recurrent VGLL2-related fusions in infantile cases. *Am J Surg Pathol*. 2016;40:224–235.
3. Waldman LE, Williamson AK, Amodio JB, et al. Congenital rhabdomyosarcoma presenting as a neck mass at birth. *Case Rep Pediatr*. 2018;2018:1243436.
4. Whittle SB, Hicks MJ, Roy A, et al. Congenital spindle cell rhabdomyosarcoma. *Pediatr Blood Cancer*. 2019;66:e27935.
5. Tan GZL, Saminathan SN, Chang KTE, et al. A rare case of congenital spindle cell rhabdomyosarcoma with TEAD1-NCOA2 fusion: a subset of spindle cell rhabdomyosarcoma with indolent behavior. *Pathol Int*. 2020;70:234–236.
6. Butel T, Karanian M, Pierron G, et al. Integrative clinical and biopathology analyses to understand the clinical heterogeneity of infantile rhabdomyosarcoma: a report from the French MMT committee. *Cancer Med*. 2020;9:2698–2709.
7. Watson S, Perrin V, Guillemot D, et al. Transcriptomic definition of molecular subgroups of small round cell sarcomas. *J Pathol*. 2018;245:29–40.
8. Geoerger B, Zwaan CM, Marshall LV, et al. Atezolizumab for children and young adults with previously treated solid tumours, non-Hodgkin lymphoma, and Hodgkin lymphoma (iMATRIX): a multicentre phase 1-2 study. *Lancet Oncol*. 2020;21:134–144.
9. Leiner J, Le Loarer F. The current landscape of rhabdomyosarcomas: an update. *Virchows Arch*. 2020;476:97–108.
10. World Health Organization (WHO). *WHO Classification of Tumours: Soft Tissue and Bone Tumors*, 5th ed. Lyon, France: International Agency for Research on Cancer; 2020.
11. Rekhi B, Upadhyay P, Ramteke MP, et al. MYOD1 (L122R) mutations are associated with spindle cell and sclerosing rhabdomyosarcomas with aggressive clinical outcomes. *Mod Pathol*. 2016;29:1532–1540.
12. Maeda T, Chapman DL, Stewart AF. Mammalian vestigial-like 2, a cofactor of TEF-1 and MEF2 transcription factors that promotes skeletal muscle differentiation. *J Biol Chem*. 2002;277:48889–48898.
13. Xu J, Li Q. Review of the in vivo functions of the p160 steroid receptor coactivator family. *Mol Endocrinol*. 2003;17:1681–1692.
14. Kendall GC, Watson S, Lin XU, et al. Genetic models reveal that the novel VGLL2-NCOA2 fusion oncogene leverages embryonic programs for sarcomagenesis [abstract]. In: Proceedings of the American Association for Cancer Research Annual Meeting 2019, Atlanta, GA; Philadelphia, PA: AACR; *Cancer Res*. 2019;79(suppl):abstract 872.
15. Sumegi J, Streblow R, Frayer RW, et al. Recurrent t(2;2) and t(2;8) translocations in rhabdomyosarcoma without the canonical PAX-FOXO1 fuse PAX3 to members of the nuclear receptor transcriptional coactivator family. *Genes Chromosomes Cancer*. 2010;49:224–236.
16. Agaram NP, Zhang L, Sung YS, et al. Expanding the spectrum of intraosseous rhabdomyosarcoma: correlation between 2 distinct gene fusions and phenotype. *Am J Surg Pathol*. 2019;43:695–702.
17. Karanian M, Pissaloux D, Gomez-Brouchet A, et al. SRF-FOXO1 and SRF-NCOA1 fusion genes delineate a distinctive subset of well-differentiated rhabdomyosarcoma. *Am J Surg Pathol*. 2020;44:607–616.
18. Cavazzana AO, Schmidt D, Ninfo V, et al. Spindle cell rhabdomyosarcoma. A prognostically favorable variant of rhabdomyosarcoma. *Am J Surg Pathol*. 1992;16:229–235.
19. Lundgren L, Angervall L, Stenman G, et al. Infantile rhabdomyofibrosarcoma: a high-grade sarcoma distinguishable from infantile fibrosarcoma and rhabdomyosarcoma. *Hum Pathol*. 1993;24:785–795.
20. Goldblum JR, Folpe AL, Weiss SW, eds. Enzinger and Weiss's Soft Tissue Tumors, 7th ed. Philadelphia, PA: Elsevier; 2020.
21. Butel T, Dumont B, Leruste A, et al. New born and infant soft tissue sarcomas. In: Chevreau C, Italiano A, eds. *Rare Sarcomas*. Cham, Switzerland: Springer; 2020:145–164.
22. Tallegas M, Fraitag S, Binet A, et al. Novel KHDRBS1-NTRK3 rearrangement in a congenital pediatric CD34-positive skin tumor: a case report. *Virchows Arch*. 2019;474:111–115.
23. Mentzel T, Beham A, Katenkamp D, et al. Fibrosarcomatous ("high-grade") dermatofibrosarcoma protuberans: clinicopathologic and immunohistochemical study of a series of 41 cases with emphasis on prognostic significance. *Am J Surg Pathol*. 1998;22:576–587.

24. Chicaud M, Frassati-Biaggi A, Kaltenbach S. Dermatofibrosarcoma protuberans, fibrosarcomatous variant: a rare tumor in children. *Pediatr Dermatol*. 2021;38:217–222.
25. Abbott JJ, Erickson-Johnson M, Wang X, et al. Gains of COL1A1-PDGFB genomic copies occur in fibrosarcomatous transformation of dermatofibrosarcoma protuberans. *Mod Pathol*. 2006;19:1512–1518.
26. Taylor JGT, Cheuk AT, Tsang PS, et al. Identification of FGFR4-activating mutations in human rhabdomyosarcomas that promote metastasis in xenotransplanted models. *J Clin Invest*. 2009;119:3395–3407.
27. Wu C, Chen X, Chen D, et al. Insight into ponatinib resistance mechanisms in rhabdomyosarcoma caused by the mutations in FGFR4 tyrosine kinase using molecular modeling strategies. *Int J Biol Macromol*. 2019;135:294–302.
28. Wetmore C, Boyett J, Li S, et al. Alisertib is active as single agent in recurrent atypical teratoid rhabdoid tumors in 4 children. *Neuro Oncol*. 2015;17:882–888.
29. Mosse YP, Fox E, Teachey DT, et al. A phase II study of alisertib in children with recurrent/refractory solid tumors or leukemia: Children's Oncology Group Phase I and Pilot Consortium (ADVL0921). *Clin Cancer Res*. 2019;25:3229–3238.
30. Savage J, Conley AJ, Blais A, et al. SOX15 and SOX7 differentially regulate the myogenic program in P19 cells. *Stem Cells*. 2009;27:1231–1243.
31. Lee HJ, Goring W, Ochs M, et al. Sox15 is required for skeletal muscle regeneration. *Mol Cell Biol*. 2004;24:8428–8436.
32. Beranger F, Mejean C, Moniot B, et al. Muscle differentiation is antagonized by SOX15, a new member of the SOX protein family. *J Biol Chem*. 2000;275:16103–16109.